

## Optical and Structural Properties of InAs/GaSb Nanostructures

D.W. Stokes, J.H Li, R.L. Forrest<sup>1</sup>, S.L. Ammu, J.C. Lenzi, S.C. Moss, B.Z. Noshov<sup>2,3</sup>, E.H. Aifer<sup>2</sup>, B.R. Bennett<sup>2</sup> and L.J. Whitman<sup>2</sup>

University of Houston, Department of Physics, Houston, TX, 77204, USA

<sup>1</sup>University of Houston-Downtown, Department of Natural Sciences, Houston, TX 77002, USA

<sup>2</sup>Naval Research Laboratory, Washington, DC, USA

<sup>3</sup>Current address: HRL Laboratories, LLC, Malibu, CA 90265, USA

### ABSTRACT

The nanostructures self-organized via lateral composition modulation in 140 period  $(\text{InAs})_{13}/(\text{GaSb})_{13}$  superlattices grown by molecular beam epitaxy have been studied by high-resolution x-ray diffraction and infrared absorption. Three samples were analyzed in this study; two with lateral composition modulation and one without. X-ray reciprocal space map scans were taken to determine the average morphology of the modulated structures. Both vertical and lateral satellite peaks were observed for the samples with composition modulation, indicating the formation of two-dimensional nanowire arrays. The vertical wavelength measured for the two samples was twice the period intended by the growers. This is due to the face-centered cubic type stacking of the nanowires. Infrared absorption spectra of these two samples were compared to the spectra of the sample with no lateral composition modulation. Transitions involving the heavy- and light-hole bands in the GaSb hole quantum well and the electron subbands of the InAs electron quantum well were not evident for the samples with lateral composition modulation, indicating that the nanostructure of the lateral composition modulation affects the optical response of the sample, which is important for optoelectronic device applications.

### INTRODUCTION

Type-II InAs/GaSb superlattices (SL) have demonstrated the unique ability to provide optical bandgaps over a wavelength range from 3-30  $\mu\text{m}$ . With the valence band of GaSb higher in energy than the conduction band of InAs, a superlattice composed of thin layers of these materials results in alternating square well potentials for holes and electrons. When the quantum confinement effects of these wells overcome the negative gap of the bulk bandstructure, without fully localizing carriers in the wells, an artificial narrow gap semiconductor is created. The bandgap (and dispersion) of the superlattice is controlled by the thickness of the InAs and GaSb layers, and the composition of the interfaces. The additional properties of reduced Auger recombination and tunneling rates relative to other material systems with comparable bandgaps have resulted in great interest in the InAs/GaSb system for applications as lasers and detectors from the mid to very long-wave IR<sup>1-7</sup>. Much investigation, however, is needed on basic materials issues, such as anion intermixing, interfacial roughness, as well as phenomena leading to the structural instability which is the subject of the present study, described below.

Recently, lateral composition modulation (LCM) was observed in InAs/GaSb superlattices<sup>8,9</sup>. LCM, which refers to the formation of phase-separated, periodic structures perpendicular to the growth direction<sup>10</sup>, induces changes in the physical properties of the material, i.e.,

increases/decreases the bandgap and affects the polarization anisotropies. Generally, LCM is avoided in device structures; however, LCM combined with the unusual band line up of the InAs/GaSb superlattice system may lead to unique characteristics that may be beneficial for optoelectronic devices, in particular, quantum wire based detectors and lasers<sup>6,7,11-16</sup>.

Theoretical subband calculations using a finite element implementation of the  $\mathbf{k} \cdot \mathbf{p}$  method are shown in figure 1 for a 40 Å/40 Å InAs/GaSb superlattice intended for detector applications. The zero point energy has been taken at the maximum of the valence band edge of GaSb. The

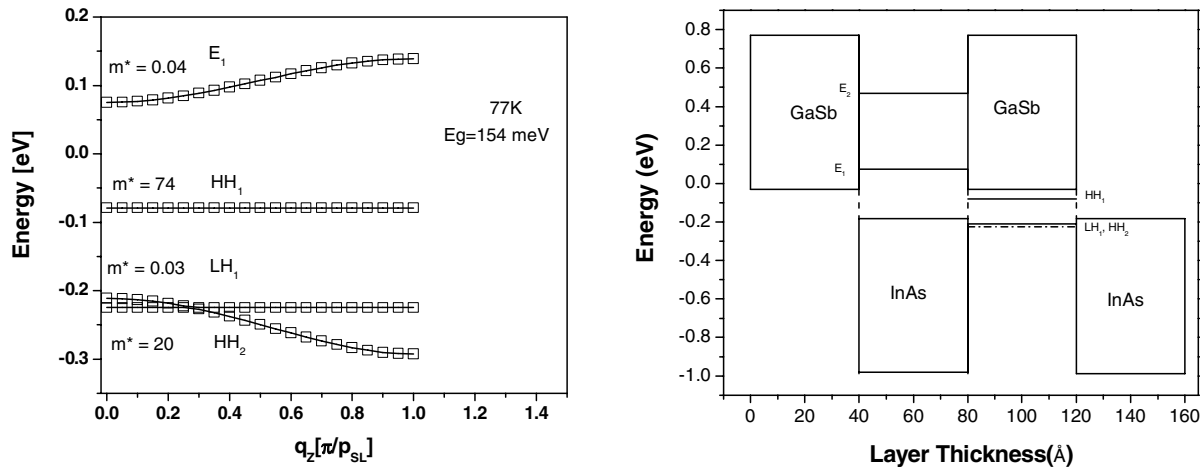


**Figure 1(a)** Calculated energy subbands for a 40 Å/40 Å InAs/GaSb superlattice and **(b)** the energy band alignments.

electron subbands,  $E_1$  and  $E_2$ , the heavy-hole subbands,  $HH_1$ ,  $HH_2$ , and the light-hole subband,  $LH_1$ , are shown. The electron, light-hole and second heavy-hole subbands show energy dispersion along the  $z$ -direction ( $q_z$ ), where  $z$  is along the growth direction and  $p_{SL}$  is the period of the superlattice. The first heavy-hole subband,  $HH_1$ , in figure 1(a) is nearly flat, indicating that the holes are almost completely localized within the GaSb layers while the non-zero  $q_z$  dispersion of the electrons,  $E_1$ , in figure 1(a), indicates that these states are extended along the growth direction. The electrons, therefore, have finite amplitude within the GaSb layers, overlapping the localized hole states and enabling optical transitions from the  $HH_1$  subband. The presence of LCM is expected to alter the SL bandstructure with the additional modulation of the potential in the plane of the superlattice layers, inducing further energy splitting and anisotropies.

In this paper we will present the results of an investigation of the structural and optical properties of LCM in InAs/GaSb superlattices. High-resolution x-ray diffraction and optical absorption characteristics will be discussed as well as how LCM may affect the performance of devices based on this system.

## EXPERIMENTAL DETAILS

Three 140 period  $(\text{InAs})_{13}/(\text{GaSb})_{13}$  superlattice structures were grown by molecular beam epitaxy (MBE) with both InAs and GaSb layers being nominally 40 Å. The SL's were intentionally grown with InSb interfacial bonds and details of the growth are given elsewhere<sup>17</sup>. Samples A and C were grown on GaSb (001) substrates and sample B was grown on a Te-doped GaSb (001) substrate. Samples A and B were grown using  $\text{As}_4$  and LCM is present. Sample C was grown using  $\text{As}_2$  and no LCM is present since the formation of LCM has been shown to be directly related to growth using  $\text{As}_4$ <sup>17</sup>. Sample A and B were grown under similar growth conditions and are identical in structure; however, the individual InAs and GaSb layers for sample A are doped (for detector purposes) while the individual layers of sample B were not doped.<sup>17</sup>

High-resolution x-ray diffraction (XRD) measurements of sample A and C were performed on a four-circle diffractometer using  $\text{Cu K}\alpha_1$  radiation ( $\lambda = 1.54041 \text{ \AA}$ ) from a 12 kW rotating anode while sample B was measured at the National Synchrotron Light Source with x-rays of energy of 8.0 keV ( $\lambda = 1.551 \text{ \AA}$ ). Normal incidence infrared absorption measurements were performed at room temperature using a Bruker Fourier transform (FTIR) spectrometer in transmission mode. The spectra were normalized and the background due to the substrate was subtracted.

## RESULTS AND DISCUSSION

X-ray reciprocal space maps (RSMs) were taken about the  $(004)$ ,  $(\bar{4}\bar{4}\bar{4})$ ,  $(002)$  and  $(\bar{2}\bar{2}\bar{4})$ , Bragg peaks perpendicular ( $\phi = 0^\circ$ ) and parallel ( $\phi = 90^\circ$ ) to the direction of the LCM. The  $\phi = 90^\circ$   $(004)$  and  $(\bar{4}\bar{4}\bar{4})$  RSMs for sample A, figures 2, shows satellite peaks corresponding to both the vertical and lateral structure. The vertical superlattice peaks, lying along the dashed line, are tilted with respect to  $(001)$  plane (solid line). This measured tilt of  $7.5^\circ \pm 0.5^\circ$  does not affect the SL crystalline planes, i.e., the  $\text{SL0}$  peak is not tilted with respect to the GaSb peak; therefore, the SL is fully strained to the substrate. Also, the vertical SL wavelength for sample A,  $\Lambda_{SL}^A = 155 \pm 10 \text{ \AA}$ , is nearly twice the 80 Å period intended by the growers. The tilt and period doubling are directly related to the face-centered cubic (fcc) like stacking of the nanowires, which is shown in the cross section scanning tunneling microscopy (XSTM) image, figure 3. This stacking is directly related to the fact that the InAs layer undulates more than the GaSb layers and because the GaSb prefers to grow between a trough and a crest of the InAs layer. The LCM wavelength, determined from the lateral satellites, (dotted lines in figure 2(a)), is  $\Lambda_{LCM}^A = 554 \pm 3 \text{ \AA}$ . This is in excellent agreement with the 600 Å spacing for the period of the<sup>18</sup> contrasting vertical bright and dark regions in the XSTM image. This contrast is due to the difference in local strain state in the two regions and indicates the InAs-rich and GaSb-rich regions, respectively. The LCM wavelength is half the period of the undulation wavelength, 1200 Å, as seen in figure 3, where typically, the LCM and undulation wavelengths are the same. Theoretical fits to XRD data determined the limiting values for the average composition of the lateral regions as well as that of the individual superlattice layers. From this fit, it was determined that alloying (anion intermixing) occurs in the individual layers with up to 12% Sb in the InAs superlattice layers and up to 4% As in the GaSb superlattice layers. Such anion cross-

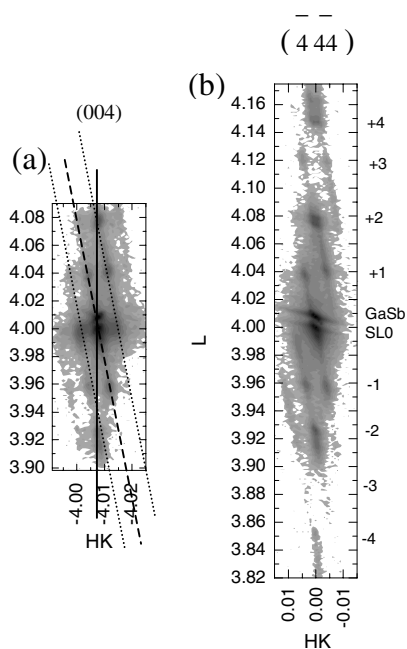


**Figure 2.** XRD reciprocal space map about the (a) (004) and (b)  $(\bar{4}\bar{4}4)$  parallel to the LCM.

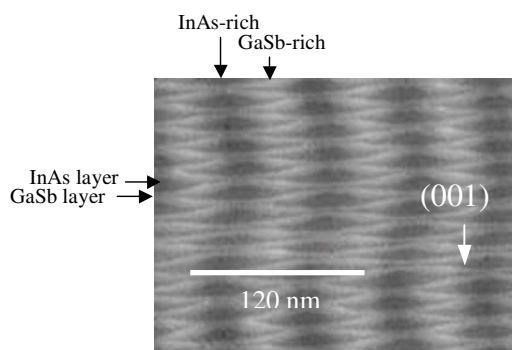


**Figure 3.** XSTM image of Sample A. The bright and dark vertical regions indicate the GaSb-rich and InAs-rich regions, respectively.

incorporation can be seen on the atomic-scale in XSTM images of the sample.<sup>9</sup> With these compositions, the InAs(Sb) layers would be under compressive strain and the Ga(As)Sb layers under tensile strain. With no alloying, InAs would be under tensile strain and GaSb would be unstrained. If the strain states of the superlattice layers are altered due to alloying, it may be one of the contributing factors to the InAs layers undulating more than the GaSb layers.

For sample B, the  $\phi = 90^\circ$  (002) and  $(\bar{2}\bar{2}4)$  RSMs, figures 4, shows up to six satellite peaks

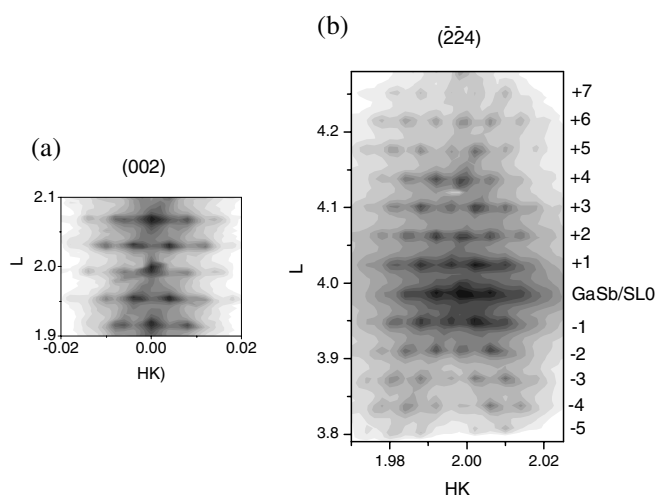


**Figure 4.** XRD reciprocal space map for sample B about the (a) (002) and (b)  $(\bar{2}\bar{2}4)$  Bragg peaks parallel to the LCM.



**Figure 5.** Atomic force microscopy (AFM) image of the top surface of sample B. InAs “wire-like” structures are formed.

corresponding to both the vertical and lateral structure. The GaSb and SL0 peak are in alignment indicating that the superlattice is fully strained to the substrate and there is no tilt for the vertical satellite peaks with respect to the (001) plane. The tilt in sample A is believed to be initiated by a very small miscut of  $0.2^\circ$ , which was measured from XRD data for the GaSb (001) substrate. Sample B was grown on a different substrate, Te doped GaSb (001) substrate, with a miscut of  $< \pm 0.1^\circ$ , measured from XRD data, which may not have been sufficient to initiate the tilting of the layers. The LCM wavelength,  $\Lambda_{LCM}^B = 617 \pm 8 \text{ \AA}$  and vertical wavelength,  $\Lambda_{SL}^B = 161 \pm 3 \text{ \AA}$  was determined from the XRD data. The similar XRD patterns for samples A and B indicate that both have a fcc-like structure for the stacking with similar LCM wavelengths (no XSTM image for sample B is available at this time). A detailed theoretical fit to the XRD data, in progress, is necessary to determine the complete extent of the LCM as well as the strain state of the system. An atomic force microscopy image of the surface of sample B, figure 5, shows InAs “wire-like” structures formed along the (110) direction, which are approximately  $1200 \text{ \AA}$  in width and several microns in length. These InAs nanowires include two LCM periods similar to the undulating wavelength of sample A. The fact that the  $\Lambda_{LCM}$  is half the undulating wavelength and the altered state of the strain of the superlattice layers will be key in characterizing the optical response of the system.

Room temperature absorption spectra for the three samples are shown in figure 6. For sample C, with no LCM, signature transitions from the  $HH_1 - E_1$ ,  $LH_1 - E_1$  and  $HH_1 - E_2$  states are clearly observed. For samples A and B, the absorption edge is shifted to higher energies and the peaks corresponding to individual transitions are no longer evident. The differences in the spectral features may be due to (1) LCM formation; (2) inhomogenities in LCM period, which are clearly seen in the XSTM images for the entire height of sample A<sup>8</sup>; (3) strain state of the system; (4) actual structure of the LCM, i.e., individual wire-like structure contains two LCM periods; or (5) fcc-like stacking of the layers. Any one or a combination of these causes can alter the band alignment, hence, the optical response of the system. The samples were designed to have a cutoff wavelength of  $8 \text{ \mu m}$ ; however, the cutoff wavelength of the samples varies. Note the peak at  $0.35 \text{ eV}$  for sample A is due to residue from thermal grease used for low temperature analysis. These

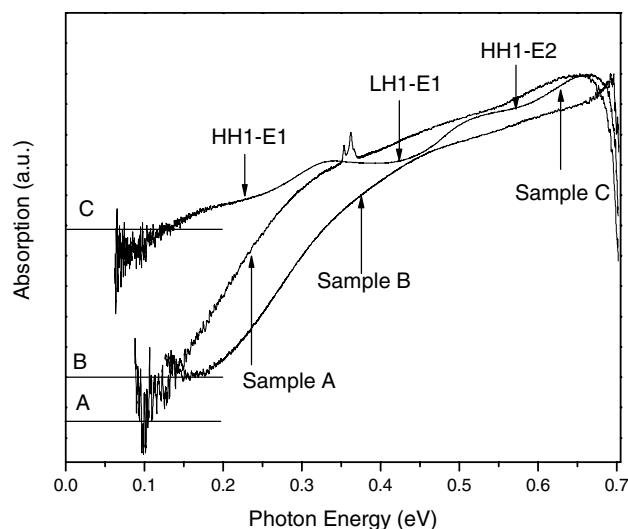


**Figure 6.** Room temperature absorption versus photon energy for samples A, B and C. Sample C, with no LCM, shows signature transitions, while these transitions are smeared for samples A and B with LCM.

preliminary absorption results do indicate that the optical response of the system has been altered; however, further analysis using polarization photoluminescence (PPL) is necessary to

sort out the reasons for the differences in the spectra. By employing PPL, 1-D confinement can clearly be demonstrated since the intensity for polarization parallel to LCM will be enhanced in comparison to the intensity for perpendicular polarization, and energy shifts and contributions due to strain can also be determined.

Impact of LCM on device performance is the subject of ongoing investigations. It is clear that the LCM has affected the optical response of the material; however, the extent of its effects, i.e., contributions due to strain and LCM, will have to be analyzed further to assess its effects on device performance.

## ACKNOWLEDGEMENTS

Research at the University of Houston is supported by the National Science Foundation on grants DMR-0099573, DMR-0237811 and DMR- 0336337, the Texas Center for Superconductivity and Advanced Materials (TcSAM) through the state of Texas and the University of Houston New Faculty Research Program. Research at Naval Research Laboratory was supported by the ONR and DARPA.

## REFERENCES

- 1 H. K. Choi, *Rev. Laser Eng.*, **25**, 14 (1997).
- 2 D. W. Stokes, L. J. Olafsen, W. W. Bewley, I. Vurgaftman, C. L. Felix, E. H. Aifer, J. R. Meyer, and M. J. Yang, *J. Appl. Phys.*, **86**, 4729 (1999).
- 3 W. W. Bewley, H. Lee, I. Vurgaftman, R. J. Menna, C. L. Felix, R. U. Martinelli, D. W. Stokes, D. Z. Garbuzov, J. R. Meyer, M. Maiorov, J. C. Conolly, A. R. Sugg, and G. H. Olsen, *Appl. Phys. Lett.*, **76**, 256 (2000).
- 4 E. H. Aifer, E. M. Jackson, G. Boishin, L. J. Whitman, J. R. Meyer, J. C. Culbertson, and B. R. Bennett, *Appl. Phys. Lett.*, **82**, 4411 (2003).
- 5 F. Fuchs, U. Weimer, W. Pletschen, J. Schmitz, E. Ahlswede, M. Walther, J. Wagner, and P. Koidl, *Appl. Phys. Lett.*, **71**, 3251 (1997).
- 6 J. C. Culbertson and B. R. Bennett, *Appl. Phys. Lett.*, **82**, 4411 (2003).
- 7 Y. Wei, A. Gin, M. Razeghi, and G. J. Brown, *Appl. Phys. Lett.*, **81**, 3675 (2002).
- 8 D. W. Stokes, R. L. Forrest, J. H. Li, S. C. Moss, B. Z. Nosh, L. J. Whitman, and M. Goldenberg, *J. Appl. Phys.*, **93**, 311 (2002).
- 9 B. Z. Nosh, B. R. Bennett, and L. J. Whitman, *Appl. Phys. Lett.*, **81**, 4452 (2002).
- 10 A. Zunger and S. Mahajan, in *Handbook on Semiconductors*, Vol. 3, 1399 (1994).
- 11 D. E. Wohlert, K. Y. Cheng, and S. T. Chou, *Appl. Phys. Lett.*, **78**, 1047 (2001).
- 12 S. T. Chou, K. Y. Cheng, L. J. Chou, and K. C. Hsieh, *J. Appl. Phys.*, **78**, 6270 (1995).
- 13 A. M. Moy, A. C. Chen, K. Y. Cheng, L. J. Chou, K. C. Hsieh, and C.-W. Tu, *J. Appl. Phys.*, **80**, 7124 (1996).
- 14 P. J. Pearah, A. C. Chen, A. M. Moy, K. C. Hsieh, and K. Y. Cheng, *IEEE J. Quantum Electron.*, **30**, 608 (1994).
- 15 Y. Arakawa and H. Sakaki, *Appl. Phys. Lett.*, **40**, 939 (1982).
- 16 A. Yariv, *Appl. Phys. Lett.*, **53**, 1033 (1988).
- 17 B. Z. Nosh, B. R. Bennett, L. J. Whitman, and M. Goldenberg, *J. Vac. Sci. Tech. B*, **19**, 1626 (2001).
- 18 R. M. Feenstra, *Physica B*, **273-274**, 796 (1999).